Title
Visualization of facet-dependent pseudo-photocatalytic behavior of TiO2 nanorods for water splitting using In situ liquid cell TEM

Authors
Yin, ZW
Betzler, SB
Sheng, T
et al.

Publication Date
2019-08-01

DOI
10.1016/j.nanoen.2019.05.068

Visualization of Facet-Dependent Pseudo-Photocatalytic Behavior of TiO_2 Nanorods for Water Splitting using In situ Liquid Cell TEM

Zu-Wei Yin,[a,b,1] Sophia Betzler,[b,1] Tian Sheng,[c,d] Qiubo Zhang,[b] Xinxing Peng,[b,c] Junyi Shangguan,[e] Karen Bustillo,[b] Jun-Tao Li,[a] Shi-Gang Sun, [a,c] Haimei Zheng, [b,e,*]

[a]*College of Energy, Xiamen University, Xiamen 361005, China*

[b]*Materials Sciences Division, Lawrence Berkeley National Laboratory, Berkeley, California 94720, United States*

[c]*State Key Lab of Physical Chemistry of Solid Surface, College of Chemistry and Chemical Engineering, Xiamen University, Xiamen 361005, China*

[d]*College of Chemistry and Materials Science, Anhui Normal University, Wuhu 241000, China*

[e]*Department of Materials Science and Engineering, University of California, Berkeley, California 94720, United States*

[*]Corresponding author.

Email address: hmzheng@lbl.gov (H. Zheng)

[1]These authors contributed equally to this work.

Abstract

We report an investigation of the pseudo-photocatalytic behavior of rutile TiO_2 nanorods for water splitting observed with liquid cell transmission electron microscopy (TEM). The electron beam serves as a "light" source to initiate the catalytic reaction and a "water-in-salt" aqueous solution is employed as the electrolyte. The observation reveals that bubbles are generated preferentially residing near the {110} facet of a rutile TiO_2 nanorod under a low electron dose rate (9.3-18.6 $e^-/Å^2$ s). These bubbles are ascribed to hydrogen gas generated from the pseudo-photocatalytic water splitting. As the electron beam current density increases to 93 $e^-/Å^2$ s, bubbles are also found at the {001} and {111} facets as well as in the bulk liquid solution, demonstrating the dominant effects of water electrolysis by electron beam under higher dose rates. The facet-dependent pseudo-photocatalytic behavior of rutile TiO_2 nanorods is further validated using density functional theory (DFT) calculation. Our work establishes a facile liquid cell TEM setup for the study of pseudo-photocatalytic water splitting and it may also be applied to investigation of other photo-activated phenomena occurring at the solid-liquid interfaces.

Key words: in situ TEM, liquid cell TEM, photocatalysis, water splitting, facet-dependent behavior

1. Introduction

Photocatalytic water splitting has attracted a lot of attention in recent years, since it converts sunlight into clean energy of hydrogen gas. TiO_2 has been widely studied as the active photocatalyst for water splitting, due to its high photocatalytic activity, superior chemical stability and non-toxicity.[1] TiO_2 is a wide-gap semiconductor which exists in many different polymorphs -- rutile, anatase being the most common ones. A large variety of anatase and rutile TiO_2 nanostructures has been synthesized for improved catalytic activities.[2] Since the catalytic reaction only takes place when the photon-induced electrons and holes are available on the surface, significant effort has been made to understand the facet dependent photocatalytic behavior of TiO_2 nanostructures.[3] First principles calculations indicated that the (101) facet of anatase structure facilitate the reduction reaction while oxidation reactions are preferred on the {001} facet.[4] These were proved by some experimental studies.[5-6] For instance, reductive (101) facets along with oxidative {001} is important for charge separation to enhance photo-degradation of methyl orange.[6] For rutile nanostructures, both {111} and {001} facets seem to promote oxidation reactions, while reductive properties were found for the {110} facets.[7-8] So far, most of the experimental studies were achieved either by monitoring the assemble activity of nanocrystals with different morphologies or through indirect characterizations, such as, the formation of Pt ($Pt^{4+} \rightarrow Pt^0$; reductive) or PbO_2 ($Pb^{2+} \rightarrow Pb^{4+}$, oxidative) nanoparticles on different TiO_2 facets.[6-8]

In situ liquid cell transmission electron microscopy (TEM) has become a powerful tool for the study of liquid-phase reactions and the dynamic phenomena at solid-liquid interfaces. [9-11] It was recently reported that UV light can be introduced into a liquid cell for the study of photo-induced water splitting by TiO_2 nanoparticles. It showed that a self-hydrogenated shell, generated around the

TiO_2 nanoparticle under UV irradiation, can promote photocatalytic H_2 evolution.[12] To limit the electron beam effects, the beam had to be blanked during the UV exposure. Thus, it would be a challenge to directly observe the facet-dependent photocatalytic behavior in real time. The work by Roy et al.[13] and Kolmakova et al.[14] demonstrated that inelastic scattering of the electron beam can initiate pseudo-photocatalytic reactions on TiO_2 surfaces similar to the ones induced by UV light. Therefore, the electron beam may be used as the "light" source to generate electron-hole pairs, featuring the opportunity to observe pseudo-photocatalytic behavior.

Here, we investigate the facet-dependent pseudo-photocatalytic activity of rutile TiO_2 nanorods for water splitting with a facile in situ liquid cell TEM setup. Rutile TiO_2 nanorods in a "water-in-salt" solution are encapsulated in a carbon-film liquid cell.[35] Different electron beam dose rates are explored to initiate the water splitting. We find that under a low electron beam dose rate, the facet-dependent pseudo-photocatalytic reactions on the surface of rutile TiO_2 nanorods can be achieved. We further conduct theoretical calculation to confirm the experimental observations.

2. Experimental Section

2.1 Synthesis and materials preparation

The raw materials, hydrochloric acid (36.5 - 38% by weight), titanium butoxide (97%), lithium bis(trifluoromethane sulfonyl) imide ($LiN(SO_2CF_3)_2$, LiTFSI) (>99.95%) were purchased from Sigma-Aldrich. Rutile TiO_2 was synthesized by a hydrothermal method, as reported elsewhere.[26] LiTFSI was firstly weighed in glove box, then de-ionized water was added to make the 21 M LiTFSI (mol-salt in kg-solvent) "water-in-salt" solution.[18]

2.2 Liquid cell preparation

Rutile TiO_2 nanorods were firstly dispersed in ethanol, then dropped on copper grids with a thin carbon film and dried at 150 ℃ for 20 min. A droplet (0.5-1μL) of the as-synthesized solution (21 M LiTFSI or pure water) was subsequently dropped on one TEM grid which was covered by another copper grid with carbon film to make a carbon/liquid/carbon sandwich structure. Then, the liquid cells were left for drying under ambient atmosphere for 1 h. Finally, the samples were transferred into a pre-vacuum system for 2 h to let the carbon film cell seal through Van der Waals force.

2.3 In situ TEM

A JEOL 2100 electron microscope operated at 200 kV was used for *in situ* observation of facet-dependent pseudo-photocatalytic behavior. The dose rates were determined after the in situ experiments in the absence of the sample by recreating the exact beam conditions used during the measurements. Characterization and statics of TiO_2 were performed using FEI Tecnai F20 and Themis 60-300 operated at 200 kV and 300 kV, respectively. The bubbles were marked in the images and assigned to different predefined regions: Region A on top of the nanowire, region B close to the nanowire surface, and region C and D in the electrolyte at different distances from the nanowire surface. The bubble area statics in videos were conducted by Matlab software based on pixel counts. The relative bubble coverage is given as ratio between bubble area in the different regions and the total size of the sub-region.

2.4 Computational methods

All electronic structure calculations were carried out using the Vienna Ab initio Simulation Package with Perdew−Burke−Ernzerhof (PBE) functional of exchange-correlation. The projector-augmented-wave (PAW) pseudopotentials were utilized to describe the core-valence

electron interaction with electrons from Ti 3p, 3d, 4s; O 2s, 2p; and H 1s shells.[27-30] The on-site Hubbard U term (DFT+ U) was added on O 2p orbitals at the value of 6.3 eV.[31] The rutile TiO_2 {110}, {111} and {001} surfaces were modeled as a p(1×1) periodic slab with four layers with 8 Ti and 16 O atoms, as shown in Figure S6. The bottom two layers were fixed and other atoms including adsorbed H_2O were relaxed during geometry optimizations. The cutoff energy was set to 500 eV and the occupancy of the one-electron states was calculated by the Gaussian smearing (SIGMA = 0.05 eV). A 6×6×1 Monkhorst−Pack k-point sampling was used and the Dipole correction was added along the z direction. The adsorption energy was defined in this work as: E_{ad} = E(water/surface) - E(surface) - E(water), where E(water/surface), E(water), and E(surface) are the total energies of the adsorbate binding to surface, free adsorbate in gas phase and clean surface, respectively.[32] The free energy of species was obtained from G = E + ZPE - TS, where E is the total energy of species, S is the entropy and ZPE is the zero point energy at room temperature. All the vibrational frequencies, v_i (Hz), were calculated based on the harmonic oscillators approximation.[33]

3. Results and Discussion

As depicted in Figure 1a, the carbon-film liquid cell is made with two commercial carbon-coated TEM grids (film thickness 10 nm) encapsulating a liquid thin film. The surface of carbon films are first activated with ozone plasma. Then, a droplet of the "water-in-salt" $LiN(SO_2CF_3)_2$ (LiTFSI) aqueous solution or pure water solution containing rutile TiO_2 nanorods is dropped onto one carbon film and it is covered with the second carbon film. The subsequent evaporation of water and the van der Waals forces seal a small amount of solution between the two carbon films. A detailed description of the rutile TiO_2 nanorod synthesis, the preparation of the aqueous "water-in-salt"

$LiN(SO_2CF_3)_2$ (LiTFSI) solution, and the liquid cell fabrication can be found in the Experimental Section.

The TiO_2 nanorods are 70-80 nm in diameter and 500-600 nm long. The ends of a nanorod show sharp tips (Figure 1b, c). The high resolution images confirm the rutile structure and reveal that a nanorod exposes the {110} facets at its sides and the tips are dominated by the {111} facets, see Figure 1d as an example. Static analysis confirms that all rutile nanorods expose the {110} facets on the sides and {111} facets at the tip, but not all have the {001} facets at the front of their tips (Fig S1).

Under a low electron dose rate of 9.3 $e^-/Å^2 \cdot s$, bubbles can be found on the side of nanorods, but there are no bubbles at the tip facets, even under the prolonged reaction times (70s) (Figure 2a, Movie S1). The bubble evolution is analyzed to show the projected area of bubbles as a function of the reaction time. As illustrated in Figure 2b, the bubble area increases during the initial 30 seconds of the electron beam exposure. After that the bubble area decreases, which is attributed to the collapse of bubbles (Figure 2a, Movie S1). As can be seen in Figure 2c, the bubble in lower left quarter of the TEM series shrinks with the time evolution. This is likely due to an increase of solvated electrons during the prolonged electron beam irradiation (i.e., from the inelastic scattering of the electron beam), which can accumulate on the surface of nanobubbles. The excessive negative surface charges destabilize the nanobubbles.[34] The collapse of nanobubbles has also been observed in previous studies.[15-16] However, as the electron beam dose rate significantly increases (see more details in Figure 3 as below), the growth of bubbles overcomes the shrinking of the bubbles, which is likely because of the enhanced pseudo-photocatalytic water splitting behavior.

To explore the effect of electron dose rate on the bubble generation behavior, different dose rates

are applied. Characteristic TEM images of the TiO_2/aqueous solution system acquired at dose rates of 18.6 $e^-/Å^2$ s and 93 $e^-/Å^2$ s are displayed in Figure 3a and c, respectively. The corresponding dynamic bubble generation behavior can be seen in Movie S2, in which the electron dose is increased from 18.6 $e^-/Å^2$ s to 93 $e^-/Å^2$ s at 40 s. At a dose rate of 18.6 $e^-/Å^2$ s, the bubbles are still predominantly formed adjacent to the {110} side facets of the TiO_2 nanorod. However, in contrast to the low dose experiment (9.3 $e^-/Å^2$ s) as described before, bubbles are also found in the bulk solution. This effect becomes much stronger at a dose rate of 93 $e^-/Å^2$ s, where the bubble concentration in the bulk solution increases significantly and bubbles are found at both the tip and sides of the nanorod. The kinetics of bubble formation is analyzed by subdividing the TEM images into two regions: Region I comprises the TiO_2 nanorod and the electrolyte close to its surface and Region II covers the bulk solution in the rest of the image. The relative bubble coverage for each region is evaluated by the ratio of bubble area to the total area. More details of the measurements for Region II (further divided into three sub-regions) are shown in Figure S2a. The bubble formation kinetics in the two regions is also analyzed under different dose rates (Figure 3b, d). Under an electron dose rate of 18.6 $e^-/Å^2$ s, the relative bubble coverage close the nanorod in Region I increases during the first 15 seconds before reaching a steady state with around 20% coverage. The bubble concentration in Region II of the bulk solution is distinctly lower, but shows a continuous increased from 1% to 8% during the course of experiment. When the electron dose rate is increased to 93 $e^-/Å^2$ s, the relative bubble coverage in Region I is jumped from 21% to 59% in 15 seconds. Simultaneously, the bubble coverage in Region II increases to 31%. Additionally, the fine analysis shows that there is no obvious variation with the Region II (Figure S2b). Under all dose rates the relative bubble coverage is significantly higher close to the TiO_2 nanorod than in

the bulk solution.

To study the bubble generation behavior at different facets under high electron dose, a quantitative analysis was performed of the relative coverage of the different facets for distinct points of time during the in situ experiments (Table S1). It becomes obvious that at low dose rates of 18.6 $e^-/Å^2s$ we do not observe bubble formation at the tip facets ({001} and {111}), while the coverage of the {110} continuously increases. At higher dose rates of 93 $e^-/Å^2s$, we first see an incomplete coverage of the tip facets which rapidly increases. After 10 s a complete coverage of the tip facets is achieved and simultaneously the coverage of the {110} facets likewise approaches 100%.

To investigate the role of aqueous "water-in-salt" solution in the facet-dependent bubble generation behavior, a solution of TiO_2 nanorods in pure water is studied as comparison. Figure 4a shows a typical TEM image of TiO_2 in pure water using the low electron dose of 9.3 $e^-/Å^2$ s, which is drastically different from that of TiO_2 in an aqueous "water-in-salt" solution (Figure 4b). In contrast to what is observed for the "water-in-salt" solution, where bubbles only form on the surface of the TiO_2 nanorods, in pure water bubbles are generated on the TiO_2 surface as well as in the bulk solution (Movie S3 and Movie S1). As depicted in Figure 3a, b and similar to the analysis described for Movie S2, each frame of Movie S3 and S1 was subdivided into the TiO_2 related region I and the bulk solution region II (which is further subdivided into region B, C, and D for Movie S3, Figure S3a). For TiO_2 nanorods in pure water, the relative bubble coverage initially increases rapidly for both regions before reaching a steady-state (Figure 4c). A slight decrease of the coverage towards the end of the movie is assigned to the collapse of part of bubbles.[15-16] The relative bubble coverage is lower in the TiO_2 related region I compared to that in the bulk solution, which arises from that bubbles on top of / below the TiO_2 nanorod are invisible. If we subtract the nanorod area from

region I we find a similar bubble concentration on the surface of the nanorod and in the bulk solution (Figure S3b). Even under the minimum electron dose required for imaging of a liquid cell in our instrument (3.1 $e^-/Å^2$ s) we find that bubbles are generated at similar rates in the bulk solution as well as on the surface of the nanorod (Figure S4a, Movie S4 (electron dose was changed from 3.1 $e^-/Å^2$ s to 9.3 $e^-/Å^2$ s at 33 s)). For TiO_2 nanorods in "water-in-salt" solution, the relative bubble coverage evolution in the TiO_2 related region I shows the similar trend as that in pure water (Figure 4c). But the relative coverage rate in "water-in-salt" solution is much lower. There is no bubbles generation in bulk solution region II, which makes the relative bubble coverage keep zero.

Multiple studies reported the electrolysis of water by the electron beam during liquid cell TEM experiments resulting in the formation of bubbles due to H_2 or O_2 generation.[17] We find a clearly enhanced stability of the "water-in-salt" $Li(H_2O)_{2.5}$-TFSI solution during electron beam irradiation compared to pure water under the same electron dose rate. This agrees well with the study of Suo et al.[16] who showed a strong interaction between the $TFSI^-$ ions and the water molecules in the $Li(H_2O)_{2.5}$-TFSI structure resulting in an enlarged electrochemical stability window of ~3 V compared to H_2O (1.23 V).[18] Hence, the use of the "water-in-salt" solution is essential for this study to avoid the vigorous reaction of the electron beam with pure water.

Inelastic scattering of the electron beam in solids features a variety of excitations including interband transitions,[19] such as transitions from the valence to the conduction band or to higher energy states. Therefore, the electron beam may act as a "light" source and generate electron-hole pairs which subsequently participate in the pseudo-photocatalytic reactions.[13-14] Our findings demonstrate that the pseudo-photocatalytic water splitting reactions on the TiO_2 nanorod surface exceeds the radiolysis of the electrolyte in a range of electron dose rates, when the "water-in-salt"

solution instead of pure water is used. From above, we can conclude that rutile TiO_2 nanorods promote the bubble generation and a facet-dependent activity is discovered with bubbles preferentially forming at the {110} facet. We also find that the exposure time required to initiate the catalytic reaction by the electron beam is much shorter (seconds) than that using the UV light in the previous photocatalytic water splitting in a liquid cell (>10 hours).[12]

A schematic illustration of facet-dependent pseudo-photocatalytic behavior on the surface of rutile TiO_2 nanorods is shown in Figure 5. The {110} facets at the side and the {111} facets at the tip are exposed to the electron beam. Electron-hole pairs are generated inside the semiconductor TiO_2 as a result of inelastic scattering of the electron beam in the material.[19] The created electron-hole pairs subsequently diffuse to the surface of the TiO_2 to participate in the catalytic reaction.[13-14] Due to the much shorter diffusion length of activated holes (~10 nm) compared to the activated electrons (~100 nm) in rutile TiO_2,[20-21] we consider electrons are the main carrier diffusing to the TiO_2 surface.

We consequently focus our theoretic modeling on an understanding of the behavior of electrons at the different surface facets using density functional theory (DFT) calculation. A detailed description of computational methods can be found in the Experimental Section. First, the water behavior at the different TiO_2 facets is analyzed by adding one layer of water molecules on the surface Ti sites to simulate the water interface. It was found that water prefers to dissociate on the {111} (ΔG=-0.3 eV) and {001} (ΔG=-0.57 eV) facets yielding the adsorbed OH* and H* species, while dissociation is less favorable on the {110} (ΔG=0.04 eV) facet. The optimized structures and reaction energies are presented in Figure S5. Based on the most stable water states on three facets, the work functions (Φ) are calculated to be in the order of {110} (5.15 eV) < {001} (5.93 eV) < {111} (7.20 eV) (Table 1). This indicates the lowest barrier for the removal of electrons at the {110} facet

and the electrons react with protons in water to form hydrogen gas. The detailed calculation is demonstrated in Figure S6. To the best of our knowledge, this is the first time that the work function of different rutile facets in aqueous environment has been achieved with the consideration of different water states on the facets. The higher energy barrier for electrons to be removed at the {111} and {001} facets make the reductive hydrogen evolution reaction less likely at these facets. We consequently attribute the bubbles generated at the {110} facet from the pseudo-photocatalytic water splitting to hydrogen gas evolution. This is supported by previous studies that deposition of platinum nanoparticles was found at the {110} facet.[7-8,22] Similarly, oxidative properties are suggested for the {111} and {001} facets.[8,22] However, we do not observe the evolution of oxygen, which is likely due to the combination of two factors. First, both the {111} and {001} facets are stabilized by hydroxylation of the under-coordinated Ti sites, which is confirmed by our calculations and consistent with previous reports.[23] This reduces their hydrophilicity thus affecting their interaction with water molecules.[23,25] Therefore, the capability to transfer charge carriers to the water molecules is reduced featuring the decreased catalytic activities.[24] Second, since the diffusion length of the holes in TiO_2 is much shorter (e.g., 10 nm[21]), most holes may be filled by electrons generated from the inelastic scattering of the electron beam before they reach the surface.

4. Conclusions

In summary, we have designed a system of rutile TiO_2 nanorods in "water-in-salt" aqueous solution for the investigation of pseudo-photocatalytic water splitting using liquid cell TEM, where the electron beam is used as the "light" source. The higher electrochemical stability of "water-in-salt" electrolyte compared to that of pure water allows to observe bubble generation from the

pseudo-photocatalytic water splitting under a low electron dose rate, where the electrolysis of water is suppressed. Electron beam induced electrolysis of water (also featuring bubble generation) is observed at higher electron dose rates.

Real time observation reveals the facet-dependent bubble generation on the {110} facet surface which is ascribed to pseudo-photocatalytic hydrogen evolution. The lower work function for removing electrons on the {110} facets compared to that on the {111} and {001} facets and the poor interaction of water molecules with the {111} and {001} facets are responsible for the observed facet-dependent behavior. The {110} facet exhibits the lowest energy barrier for the removal of electrons suggesting that the water reduction predominantly take place on this facet. Although the evolution of oxygen is expected on the {111} and {001} facets, but it is impeded. This is likely due to the lack of hole transfer channels due to the low hydrophilicity of respective facets. In combination with the small diffusion length of holes in TiO_2 their recombination with beam electrons is more probable than the oxidation of water.

Our study presents a new method for the pseudo-photocatalytic semiconductor/liquid interfacial behavior using in situ TEM, at which real time imaging can yield profound insights into photocatalytic mechanisms.

Acknowledgements

This work was funded by the U.S. Department of Energy (DOE), Office of Science, Office of Basic Energy Sciences (BES), Materials Sciences and Engineering Division under Contract No. DE-AC02-05-CH11231 within the in situ TEM program (KC22ZH) program. Z. W. Yin. acknowledges the financial support from China Scholarship Council (201606310151). S.

Betzler acknowledges financial support from the Alexander von Humboldt Foundation. J. T. Li thanks the support of NSFC (21621091) and Natural Science Foundation of Fujian Province of China (2015J01063).

Conflicts of interest

There are no conflicts of interest to declare.

References

[1] A. L. Linsebigler, G. Lu, J. T. Yates, Photocatalysis on TiO_2 surfaces: principles, mechanisms, and selected results, Chem. Rev. 95 (1995) 735-758.

[2] X. Chen, S. S. Mao, Titanium dioxide nanomaterials: synthesis, properties, modifications, and applications, Chem. Rev.107 (2007) 2891-2959.

[3] K. Bourikas, C. Kordulis, A. Lycourghiotis, Titanium dioxide (anatase and rutile): surface chemistry, liquid-solid interface chemistry, and scientific synthesis of supported catalysts, Chem. Rev. 114 (2014) 9754-9823.

[4] S. Selcuk, A. Selloni, Facet-dependent trapping and dynamics of excess electrons at anatase TiO_2 surfaces and aqueous interfaces, Nat. Mater. 15 (2016) 1107-1113.

[5] J. Pan, G. Liu, G. Q. Lu, H. M. Cheng, On the true photoreactivity order of {001}, {010}, and {101} facets of anatase TiO_2 crystals, Angew. Chem. Int. Edi. 123 (2011) 2181-2185.

[6] N. Roy, Y. Sohn, D. Pradhan, Synergy of low-energy {101} and high-energy {001} TiO_2 crystal facets for enhanced photocatalysis, ACS nano 7 (2013) 2532-2540.

[7] T. Ohno, K. Sarukawa, M. Matsumura, Crystal faces of rutile and anatase TiO_2 particles and their roles in photocatalytic reactions, New J. Chem. 26 (2002) 1167-1170.

[8] E. Bae, T. Ohno, Exposed crystal surface-controlled rutile TiO_2 nanorods prepared by hydrothermal treatment in the presence of poly (vinyl pyrrolidone), Appl. Catal., B-Environ. 91 (2009) 634-639.

[9] H. Zheng, R. K. Smith, Y. W. Jun, C. Kisielowski, U. Dahmen, A. P. Alivisatos, Observation of single colloidal platinum nanocrystal growth trajectories, Science 324 (2009)1309-1312.

[10] H. G. Liao, L. Cui, S. Whitelam, H. Zheng, Real-time imaging of Pt_3Fe nanorod growth in solution, Science 336 (2012) 1011-1014.

[11] H. G. Liao, D. Zherebetskyy, H. Xin, C. Czarnik, P. Ercius, H. Elmlund, L. Wang, H. Zheng, Facet development during platinum nanocube growth, Science 345 (2014) 916-919.

[12] Y. Lu, W. J. Yin, K. L. Peng, K. Wang, Q. Hu, A. Selloni, F. R. Chen, L. M. Liu, M. L. Sui, Self-hydrogenated shell promoting photocatalytic H_2 evolution on anatase TiO_2, Nat. Commun. 9 (2018) 2752.

[13] P. Roy, R. Lynch, P. Schmuki, Electron beam induced in-vacuo Ag deposition on TiO_2 from ionic liquids, Electrochem. Commun. 11 (2009) 1567-1570.

[14] N. Kolmakova, A. Kolmakov, Scanning Electron Microscopy for in Situ Monitoring of Semiconductor-Liquid Interfacial Processes: Electron Assisted Reduction of Ag Ions from Aqueous Solution on the Surface of TiO_2 Rutile Nanowire, J. Phys. Chem. C 114 (2010) 17233-17237.

[15] D. Shin, J. B. Park, Y. J. Kim, S. J. Kim, J. H. Kang, B. Lee, S. Cho, B. Hong, K. S. Novoselov, Growth dynamics and gas transport mechanism of nanobubbles in graphene liquid cells, Nat. Commun. 6 (2015) 6068.

[16] E. R. White, M. Mecklenburg, S. B. Singer, S. Aloni, B. C. Regan, Imaging nanobubbles in water with scanning transmission electron microscopy, Appl. Phys. Express 4 (2011) 055201.

[17] J. M. Grogan, N. M. Schneider, F. M. Ross, H. H. Bau, Bubble and pattern formation in liquid induced by an electron beam, Nano Lett. 14 (2014) 359-364.

[18] L. Suo, O. Borodin, T. Gao, M. Olguin, J. Ho, X. Fan, C. Luo, C. Wang, K. Xu, "Water-in-salt" electrolyte enables high-voltage aqueous lithium-ion chemistries, Science 350 (2015) 938-943.

[19] D. Williams, B. Carter, Transmission electron microscopy, Springer, Boston, MA, 1996, 50-60.

[20] Y. Yamada, Y. Kanemitsu, Determination of electron and hole lifetimes of rutile and anatase TiO_2 single crystals, Appl. Phys. Lett. 101 (2012) 133907.

[21] Y. J. Hwang, C. Hahn, B. Liu, P. Yang, Photoelectrochemical properties of TiO_2 nanowire arrays: a study of the dependence on length and atomic layer deposition coating, ACS Nano 6 (2012) 5060-5069.

[22] E. Bae, N. Murakami, T. Ohno, Exposed crystal surface-controlled TiO_2 nanorods having rutile phase from $TiCl_3$ under hydrothermal conditions, J. Mol. Catal. A-Chem. 300 (2009) 72-79.

[23] Y. Wang, T. Sun, X. Liu, H. Zhang, P. Liu, H. Yang, X. Yao, H. Zhao, Geometric structure of rutile titanium dioxide (111) surfaces, Phys. Rev. B 90 (2014) 045304.

[24] F. Liu, N. Feng, Q. Wang, J. Xu, G. Qi, C. Wang, F. Deng, Transfer Channel of Photoinduced Holes on a TiO_2 Surface As Revealed by Solid-State Nuclear Magnetic Resonance and Electron Spin Resonance Spectroscopy, J. Am. Chem. Soc. 139 (2017) 10020-10028.

[25] K. Takahashi, H. Yui, Analysis of surface OH groups on TiO_2 single crystal with polarization modulation infrared external reflection spectroscopy, J. Phys. Chem. C 113 (2009) 20322-20327.

[26] A. Folger, J. Kalb, L. Schmidt-Mende, C. Scheu, Tuning the electronic conductivity in hydrothermally grown rutile TiO_2 nanowires: Effect of heat treatment in different environments, Nanomaterials 7 (2017) 289-302.

[27] G. Kresse, J. Hafner, Ab initio molecular dynamics for open-shell transition metals, Phys. Rev. B 48 (1993) 13115-13118.

[28] G. Kresse, J. Furthmuler, Efficient iterative schemes for ab initio total-energy calculations using a plane-wave basis set, Phys. Rev. B 54 (1996) 11169-11186.

[29] P. E. Blochl, Projector augmented-wave method, Phys. Rev. B 50 (1994) 17953-17979.

[30] G. Kresse, D. Joubert, From ultrasoft pseudopotentials to the projector augmented-wave method, Phys. Rev. B 59 (1999) 1758-1775.

[31] J. Pedrew, K. Burke, M. Ernzerhof, Generalized Gradient Approximation Made Simple, Phys. Rev. Lett. 77 (1996) 3865-3868.

[32] D. Wang, T. Sheng, J. Chen, H. Wang, P. Hu, Identifying the key obstacle in photocatalytic oxygen evolution on rutile TiO_2, Nature Catal. 1 (2018) 291-299.

[33] A. Gokhale, S. Kandoi, J. Greeley, M. Mavrikakis, J. Dumesic, Molecular-level descriptions of surface chemistry in kinetic models using density functional theory, Chem. Eng. Sci. 59 (2004) 4679-4691.

[34] N. Nirmalkar, A. W. Pacek, M. Barigou, Interpreting the interfacial and colloidal stability of bulk nanobubbles, Soft matter 14 (2018) 9643-9656.

[35] Y. Wang, X. Peng, A. Abelson, P. Xiao, C. Qian, L. Yu, C. Ophus, P. Ercius, L. Wang, M. Law, H. Zheng, Dynamic deformability of individual PbSe nanocrystals during superlattice phase transitions, Science Advances (2019) in press.

Table 1. The calculated work function (Φ) for the three different facets (i.e., (100), {110} and {111}) of TiO_2 nanorods in an aqueous environment, by considering the dissociation of water molecules or without water dissociation. The water molecules without dissociation are the most stable state on the {110} facet, while the dissociated water is the most stable state on the {111} and {001} facets.

	{110}	{111}	{001}
Considering water dissociation	5.15 eV	7.20 eV	5.93 eV
No dissociation of water	5.15 eV	6.05 eV	5.21 eV

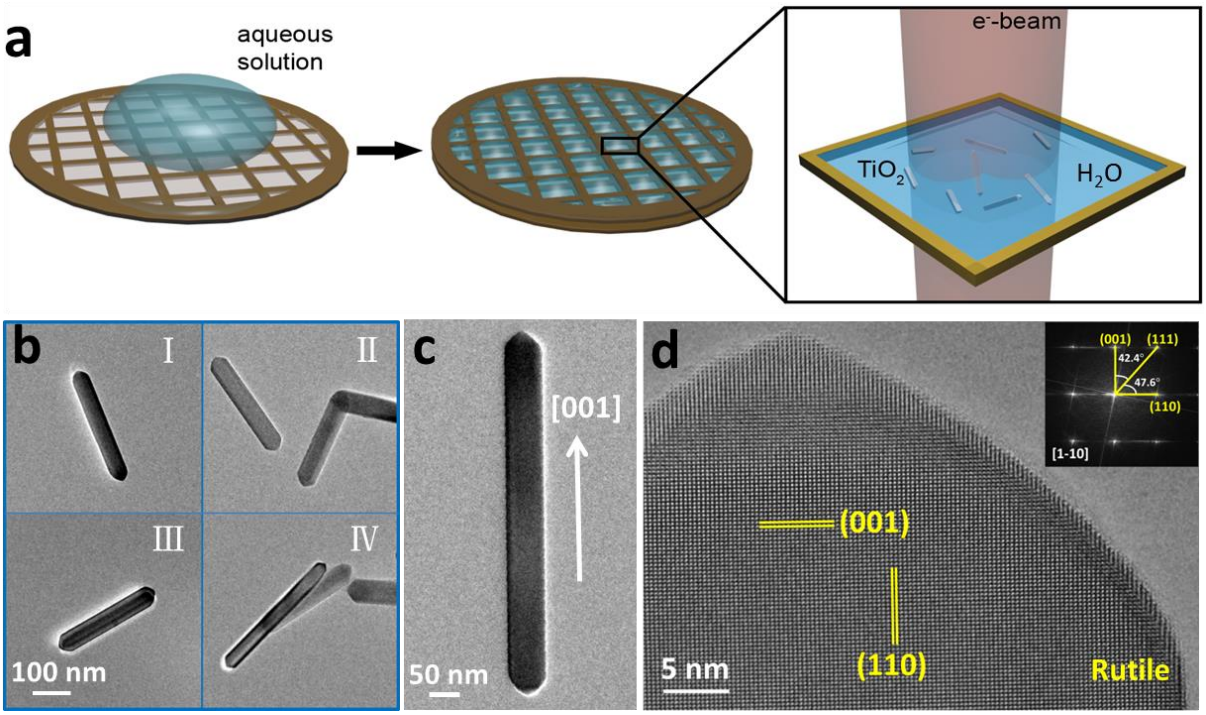

Figure 1. Preparation of a liquid cell for in situ TEM imaging of pseudo-photocatalytic water splitting by TiO_2 nanorods. (a) A schematic showing the preparation of a carbon film based liquid cell for in situ TEM imaging. (b) Low magnification TEM images of TiO_2 nanorods from different regions in a liquid cell. (c) A representative TEM image showing the long axis of a TiO_2 nanorod along the [001] direction. (d) High resolution TEM image showing the tip of a TiO_2 nanorod. Inset is a fast Fourier transform (FFT) pattern showing the rutile structure.

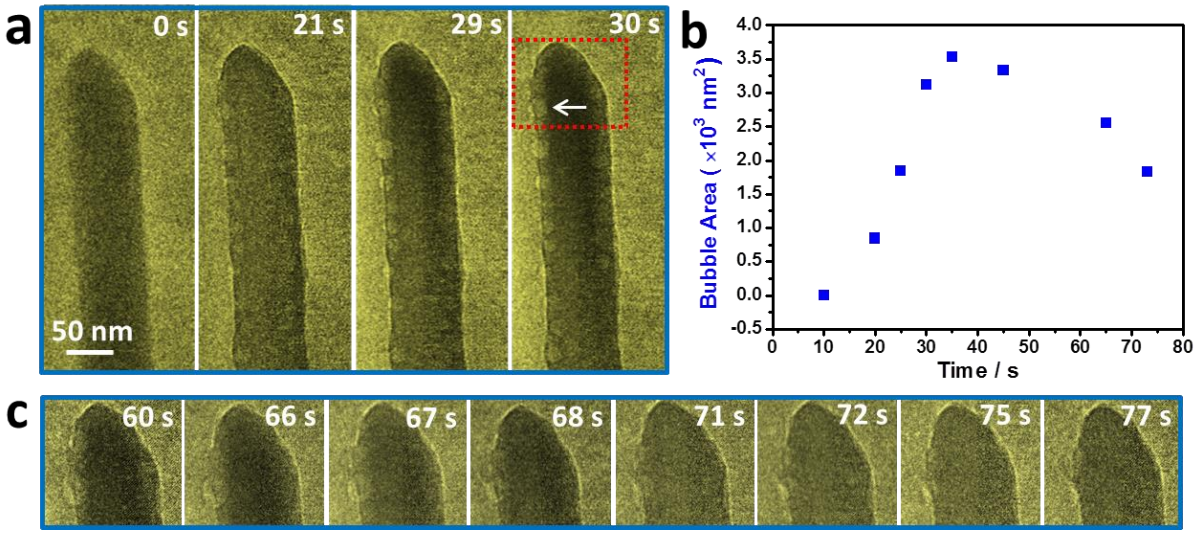

Figure 2. Real time observation of facet-dependent gas bubble generation behavior. (a) Sequential TEM images showing the facet-dependent bubble generation under an electron dose rate of 9.3 $e^-/Å^2$ s. (b) The amount of bubbles measured by the projected area of bubbles as a function of time. (c) Sequential TEM images showing the bubble collapse under an electron dose rate of 9.3 $e^-/Å^2$ s. The regions of frames are the same as red box labeled in (a).

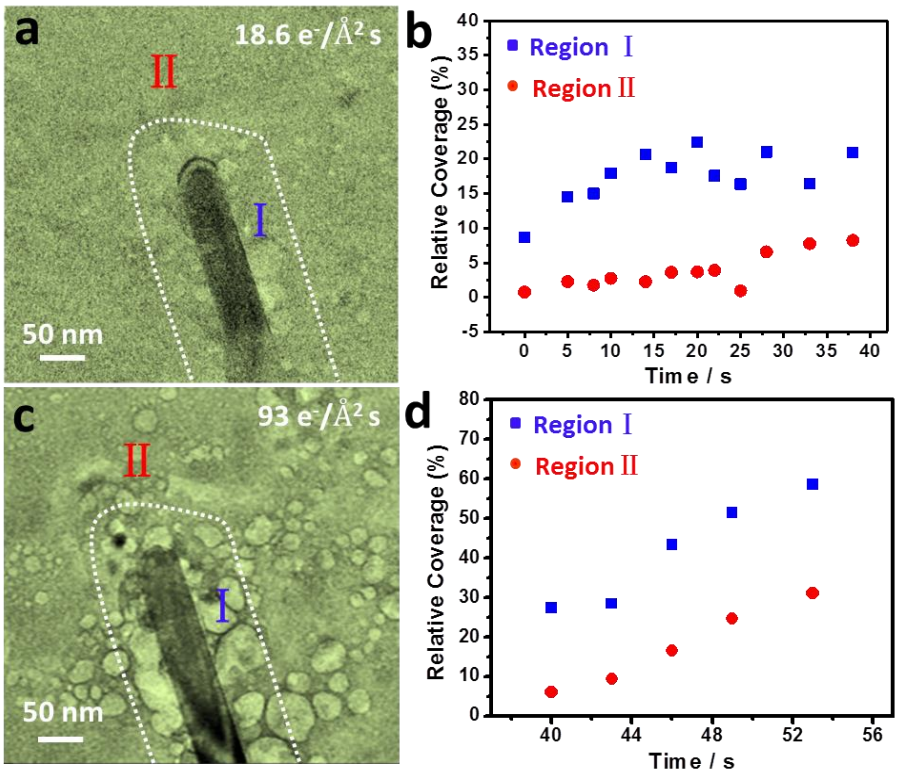

Figure 3. Electron dose effects on gas bubble generation. (a) A typical TEM image showing the bubble generation behavior under an electron dose rate of 18.6 $e^-/Å^2$ s. (b) The projected area of bubbles as a function of time in region I related to TiO_2 nanorod and in region II of the bulk solution corresponding to (a). (c) A typical TEM image showing bubble generation behavior under an electron dose rate of 93 $e^-/Å^2$ s. (d) The amount of bubbles measured by the relative coverage of bubble area as a function of time in region I and region II corresponding to (c).

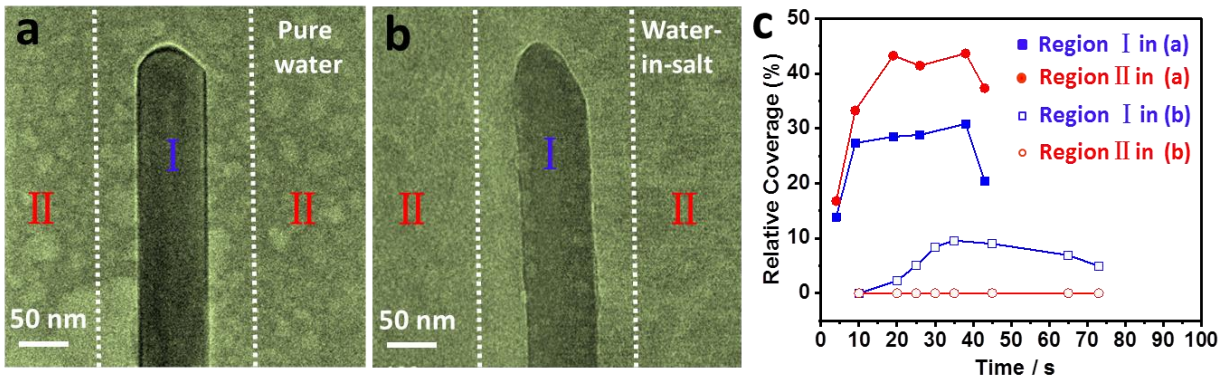

Figure 4. Role of the "water-in-salt" aqueous solution in facet-dependent bubble generation behavior of TiO_2 nanorod. (a) A typical TEM image showing the bubble generation behavior of the system of TiO_2 in pure water under an electron dose rate of 9.3 $e^-/Å^2$ s. (b) Bubble generation behavior of TiO_2 in a "water-in-salt" solution under the same electron dose rate of 9.3 $e^-/Å^2$ s. (c) The amount of bubbles measured by the relative coverage of bubble area as a function of time in region I and region II corresponding to (a) and (b).

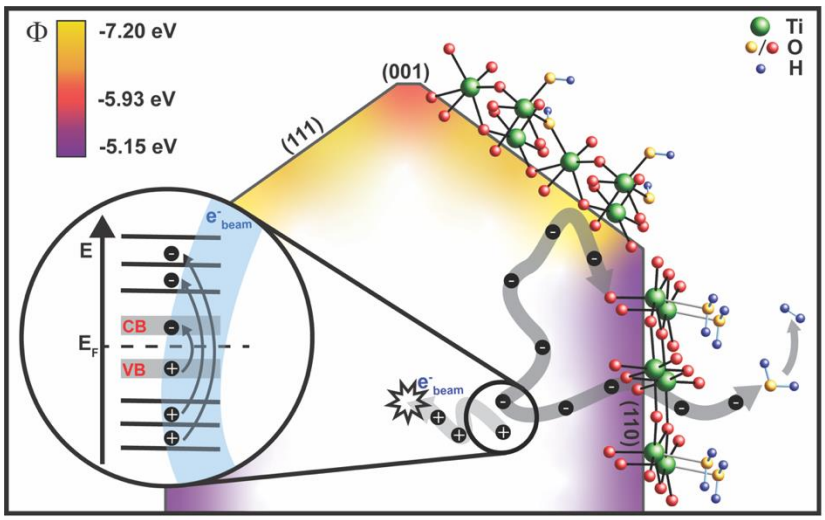

Figure 5. A schematic illustration of the proposed mechanism for the facet-dependent pseudo-photocatalytic hydrogen evolution on rutile TiO_2 nanorods in a "water-in-salt" solution under low electron dose (e.g., 9.3-18.6 $e^-/Å^2$ s).